Infrared polarisation measurements of targets and backgrounds in a marine environment

Frank Cremer[abc], Piet B.W. Schwering[a], Wim de Jong[a], Klamer Schutte[a] and Arie N. de Jong[a]

[a]TNO Physics and Electronics Laboratory, P.O. Box 96864, 2509 JG, The Hague, The Netherlands
[b]Pattern Recognition Group, Delft University of Technology, Delft, The Netherlands
[c]Section of Applied Geophysics, Delft University of Technology, Delft, The Netherlands

ABSTRACT

The infrared (IR) radiation emitted or reflected in an off-normal direction from a smooth surface is partially polarised. This principle can be used for enhanced discrimination of targets from backgrounds in a marine environment. It has been shown that (man-made) targets do not demonstrate a pronounced polarisation effect when observed from near normal direction whereas the sea background radiation has a certain degree of polarisation in slant observation path.

A measurement setup has been constructed for collecting polarised IR imagery. This setup contains a rotating polarisation filter that rotates synchronously with the frame sync of the camera. Either a long wave IR (LWIR) or a mid wave IR (MWIR) camera can be mounted behind the rotating polarisation filter. The synchronisation allows a sequence of images to be taken with a predefined constant angle of rotation between the images. Out of this image sequence three independent Stokes images are constructed, containing the normal intensity part, the vertical/horizontal polarisation and the diagonal polarisation. Upto 20 full linearly polarised images can be acquired per second.

Measurements are taken at the North Sea coast with this setup. The recorded images are analysed to determine the influence of polarisation on the detection of small targets in such an environment. Furthermore differences between polarisation contrasts in MWIR are analysed.

1. INTRODUCTION

It is well known that electro-magnetic radiation reflecting from a smooth surface observed near a grazing angle becomes (partly) polarised. This phenomenon has been shown for visual as well as infrared wavelength bands. Less known is the phenomenon that electro-magnetic radiation emitted from smooth surfaces also becomes polarised.

This polarisation phenomenon can contribute in the detection of small targets in a marine environment, see Figure 1. Radiation from the sea surface becomes polarised due to reflection or emission when observed near grazing angles. Small targets (like swimmers or a life raft) in this environment generally are observed under a different, near grazing, angle and therefore are less polarised.

The polarisation effects in a marine environment are just the opposite from land-based target detection, like land-mine detection.[11] The landmines generally exhibit a larger polarisation effect than backgrounds (soil, vegetation). This contradiction can be explained by the fact that the sea surface is relatively smooth and observed at a grazing angle, whereas most targets in this marine environment are observed at an almost perpendicular angle.

In the remainder of this section related work is discussed as well as an introduction into the theory of infrared polarisation is given. In Section 2 the measurement setup that is used to collect infrared polarised imagery is described. This setup is used to do near-shore measurements of the North Sea. The measurement conditions are described in Section 3. The acquired measurements and how infrared polarisation contributes in the detection of target is described in Section 4.

Further author information: (Send correspondence to Frank Cremer)
Frank Cremer: E-mail: Cremer@fel.tno.nl Phone: +31 70 374 0795 Fax: +31 70 374 0654

Targets and Backgrounds VII: Characterization and Representation, Wendell R. Watkins, Dieter Clement, William R. Reynolds, Editors, Proceedings of SPIE Vol. 4370 (2001)

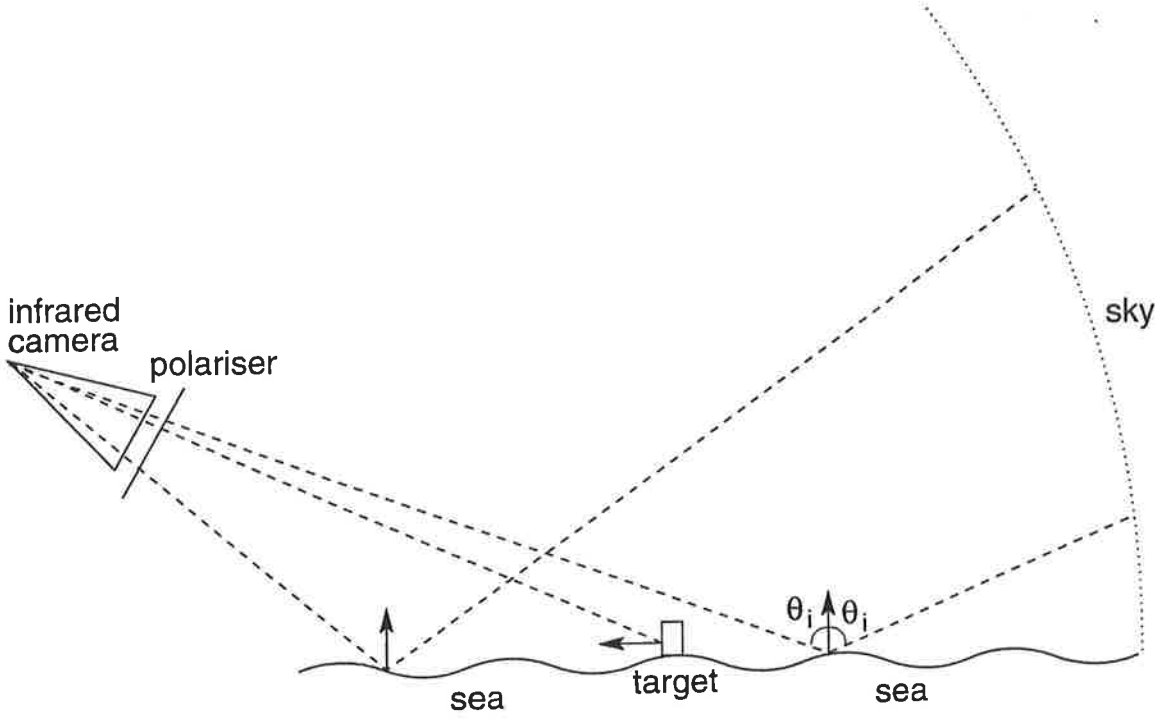

Figure 1. The TIR polarisation setup looking onto the sea and sky reflection on the sea.

1.1. Related work

Infrared polarisation measurements in a marine environment have been performed and reported previously by a number of authors. One group of authors is from the Naval Postgraduate School in Monterey (CA). This group consists of Cooper,[3–6] Gregoris[8] and Walker.[13] They all used a dual band camera (MWIR and LWIR) and a wire grid polariser. This polariser was rotated manually, giving a delay of about 10 s between measurements. There was no correction for narcism. They claim that for the MWIR polarisation the reflection dominates and that for the LWIR the emission dominates. Furthermore the measured sky polarisation was low as well as the measured polarisation of the targets.

In a different approach, Iannarilli[10] used a hyper spectral polarimetric imager for ocean sensing (wave slope retrieval).

A group of FGAN-FOM, Germany reported on the measurements with an infrared polarisation filter in a marine environment.[12] Their setup consists of a telescope and a continuously rotating polarisation filter. Images from an infrared camera (1.2 - 5.9 μm) where recorded on tape. With the filter in vertical orientation, the number of hot spots due to sun glints in the waves were reduced and targets could be more easily seen. They also measured polarised reflections from clouds.

Finally, Balfour[1] performed some initial measurements on infrared polarisation. A similar measurement setup was used as described in this paper. Measurements were taken after sun set. The image clearly shows that the sea is polarised, whereas the targets and the sky are less polarised.

1.2. Polarisation theory

Under a number of assumptions,[7] the polarised radiation of a flat surface of a target irradiated by a black body source is easily modelled. One of the assumptions is that the surface of this target (or background) is completely flat and specular for reflection. This surface has a fixed temperature T_s. Assume that a black body source with temperature T_{bb} is irradiating on this surface. The Linearly Polarised radiance LP is under this assumption (as well as a few others) given by[7]:

$$LP(T_s, T_{bb}, \theta_i) = \frac{1}{2}\text{abs}\left[(\rho_s(\theta_i) - \rho_p(\theta_i))\,(I_{BB}(T_{bb}) - I_{BB}(T_s))\right] \quad [W/m^2 sr], \tag{1}$$

with θ_i the incidence angle and $\rho_p(\theta_i)$, $\rho_s(\theta_i)$ the reflection coefficients for respectively the polarisation parallel to the plane of incidence and perpendicular to the plane of incidence. The function $I_{BB}(T)$ is the radiance over the wavelength band of the camera and is calculated by integrating Planck's equation.

Equation 1 shows that if the reflected black body source has the same temperature as the reflecting surface, the linear polarisation is zero. Furthermore, there is an angular dependency. For $\theta_i = 0$ degree, both reflection coefficients are the same and there will also be no linear polarisation. Radiation sources in the marine environment are the sun, clouds and the blue sky. These sources do not exactly behave like black bodies, so this model may not be applicable. Nonetheless, this model give insight into the phenomenon of infrared polarisation. The apparent sky temperature depends on the elevation angle of the camera and the spectral wavelength band. This temperature ranges from the ambient temperature at ground level to less than 230 K at high elevations.

The radiance originating from a particular area of the surface passes through a polariser and subsequently via the optical system onto the detector array of the camera. The detector of the camera delivers a signal proportional to the scene radiance. This value depends on the orientation of the filter. For a given angle φ between the principal axis of the polarisation filter and the horizontal axis, the measured scene radiance I_c of a detector element of the camera is given by:

$$I_c(\varphi) = \frac{1}{2}C\left[I + Q\cos(2\varphi) + U\sin(2\varphi)\right] \quad [W/m^2 sr], \tag{2}$$

where $\varphi = 0$ represents the situation that horizontal polarised radiation passes unattenuated through the linear polariser. The constant C contains all the parameters of the optical system. The parameters I, Q and U are three of the four Stokes parameters.[9] I is the total radiation, Q is the horizontal or vertical polarised radiation and U is the diagonal polarised radiation. The fourth Stokes parameter V defines the circular polarisation and is not considered in the model and cannot be measured with a linear polariser.

The above representation of polarisation defines the LP radiation LP and the polarisation angle ω:

$$LP = \sqrt{Q^2 + U^2}, \tag{3}$$

$$\omega = \frac{1}{2}\arctan(U/Q), \tag{4}$$

with ω the angle between the principal axis of the filter and the horizontal orientation. For a flat surface and a single radiation source as is assumed in the model, only two different polarisation angles are found: one in which emission polarisation dominates $\omega = 90°$ (vertical polarisation) and one in which reflection polarisation dominates $\omega = 0°$ (horizontal polarisation).

The radiance intensity as measured by the camera behind the polariser is given in Equation 2. With our polarisation setup, described in Section 2, this radiance is measured over a full rotation of the filter in N frames. The Stokes-Müller polarisation parameters $\tilde{I}$, $\tilde{Q}$ and $\tilde{U}$ are estimated by:

$$\begin{aligned}
\tilde{I} &= \frac{2}{N}\sum_{j=1}^{N} I_c(\varphi_j) \\
\tilde{Q} &= \frac{4}{N}\sum_{j=1}^{N} I_c(\varphi_j)\cos(2\varphi_j) \\
\tilde{U} &= \frac{4}{N}\sum_{j=1}^{N} I_c(\varphi_j)\sin(2\varphi_j),
\end{aligned} \tag{5}$$

with N the number of frames (in this paper either 10 or 60), j the frame number and $\varphi_j = \frac{2\pi j}{N}$ the angle of the linear polariser for frame j. The angle of the polariser has not been calibrated, so instead of directly using the Stokes parameter Q, the estimated linear polarisation $\tilde{LP}$ is used, as defined by Equation 3.

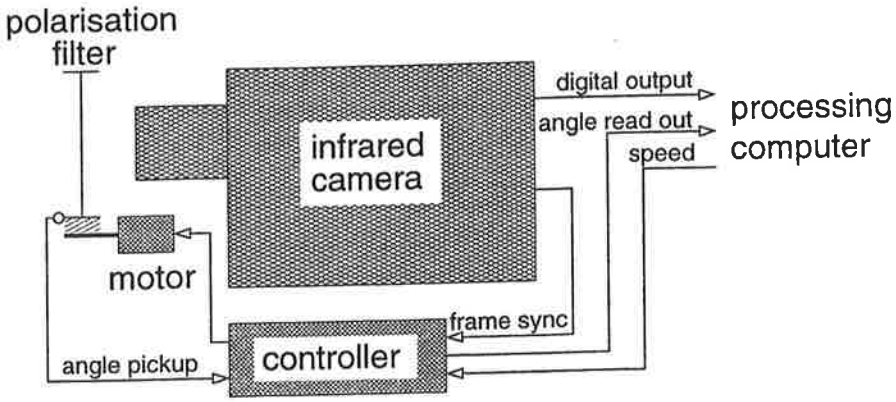

(a)

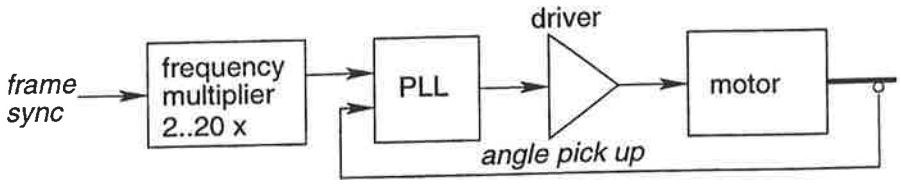

(b)

Figure 2. a) Infrared polarisation setup, consisting of a wire-grid polariser, a motor, an infrared camera and custom-made controller electronics. b) The motor controller multiplies the frame sync by a number as given by the processing computer. This is input to the Phase Locked Loop (PLL), which drives the motor so that the angle pick up has the same frequency as the multiplied frame sync. The angle pick up gives a pulse for every 3 degrees of rotation.

2. MEASUREMENT SETUP

A measurement setup is constructed for infrared polarisation measurements. This setup consists of an infrared polariser, a motor to rotate the polariser, a motor controller and a mount for the infrared camera. The polariser is applicable to both the MWIR and LWIR wavelength bands. The task of the motor controller is to rotate the polariser synchronously with the frame rate of the camera. This means that between two frame synchronisation pulses the filter is rotated over a fixed angle. This angle is presettable between 6° and 60°. Radiation from the cooled detector array, the lens and the camera housing is partly reflected by the polarisation filter. This phenomenon is called narcism and has been solved by measuring and compensating for these reflections. A more thoroughly description of this measurement setup can be found in Cremer *et al.*[7]

Only three independent measurements are necessary for a full estimation of the Stokes linear polarisation parameters in Equation 5. However taking more measurements reduces the error in the estimation. It also facilitates the evaluation of the quality of the estimation. The Root Mean Square (RMS) σ^2 of the difference between the measured radiance as function of the angle φ_i and the expected radiance in Equation 2 based on the estimated Stokes parameters $\tilde{I}$, $\tilde{Q}$ and $\tilde{U}$ from Equation 5 is given by:

$$\sigma^2 = \frac{1}{N}\sum_{i=1}^{N}\left(I_c(\varphi_i) - \frac{1}{2}\left(\tilde{I} + \tilde{Q}\cos(2\varphi_i) + \tilde{U}\sin(2\varphi_i)\right)\right)^2. \quad (6)$$

If the model fit of $\tilde{I}$, $\tilde{Q}$ and $\tilde{U}$ is close, then the model error σ^2 is an estimation of the Gaussian pixel noise. However, there are other changes in the image (for example due to movement of targets) and this will cause to give a much higher error than can be expected based on the pixel noise.

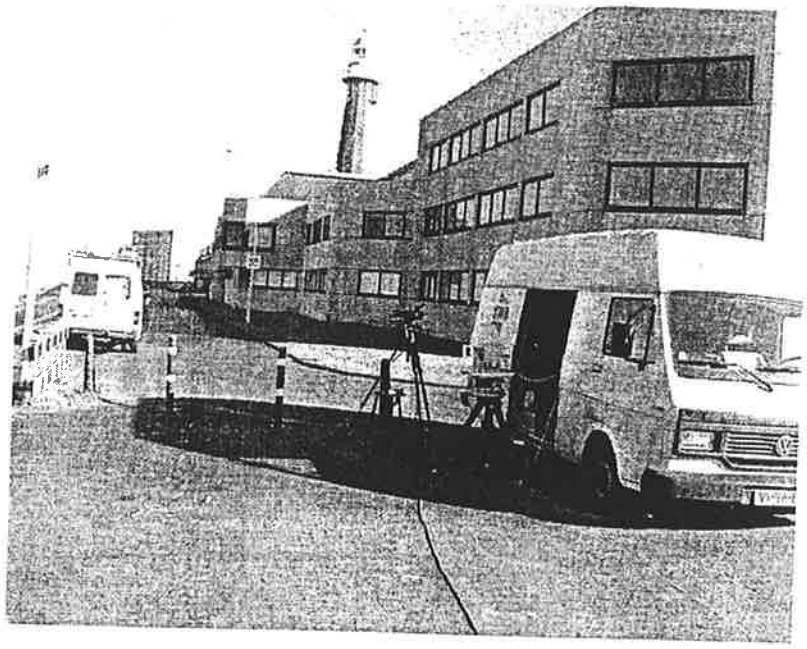

Figure 3. The measurement location at Scheveningen beach.

3. MEASUREMENT CONDITIONS

At February 25, 2001 infrared polarisation measurements were taken on the North Sea coast. The location was on top of a dike, close to the harbour of Scheveningen, the Netherlands, see Figure 3. The camera position was at a height of 18.3 m above sea level. A (visual) photo of the field of view of the infrared polarisation setup is shown in Figure 4(a). A typical (not linear polarised) MWIR image is shown in Figure 4(b).

All measurements were performed with the Radiance HS camera. This is a MWIR camera (3-5 μm). A 100 mm lens was used to acquire the images. This lens and camera combination corresponds to a Field Of View (FOV) of 4.4°. The MWIR camera has a focal plane array of 256 by 256 detectors. The instantaneous field of view for each detector was 0.3 mrad for this 100 mm lens and this camera. The f number of the optics is 2.3.

In the images of Figure 4 three buoys and a small boat are present. This small boat is not always present and also not always at the same location in the image. The first buoy (number 3) is located at the relative close distance of 943 m. The other two buoys (number 1 and 2) are at a distance of around 2300 m. At large distances, almost at the horizon, ships are passing by. However, these ships will not be included in our analyses, since we were unable to visually verify these targets.

The air temperature at noon was 7° C and the sky was almost perfectly clear. The relative humidity was 87% and there was a very mild wind from the east (less than 1 m/s). The viewing direction was looking west. The visibility over land was high, but above the sea, the visibility was much lower (a few kilometers). It was not possible to visually see the horizon. The sea state was low, due to the low wind speed. Except for the surf zone, the sea appeared completely flat. The sea temperature was 7.0° C.

4. ANALYSES AND DISCUSSION

4.1. Initial analyses

One set of polarised (and intensity) images are shown in Figure 5. In the radiance intensity image, the buoys and the ship are easily detectable. This is due to the relative short distances and the clear weather conditions. Nonetheless, we will show what polarisation can contribute in this specific case, providing insight in how it can be applicable in other situations.

In the LP image, two of the buoys and the boat are clearly visible. This is in contrary to the literature[1] . This phenomenon is explained later on. First consider the polarisation of the sea. The sea is polarised, though not completely. There are a few highly polarised patches visible. The foreground seems more polarised than the background (close to the horizon). In the intensity

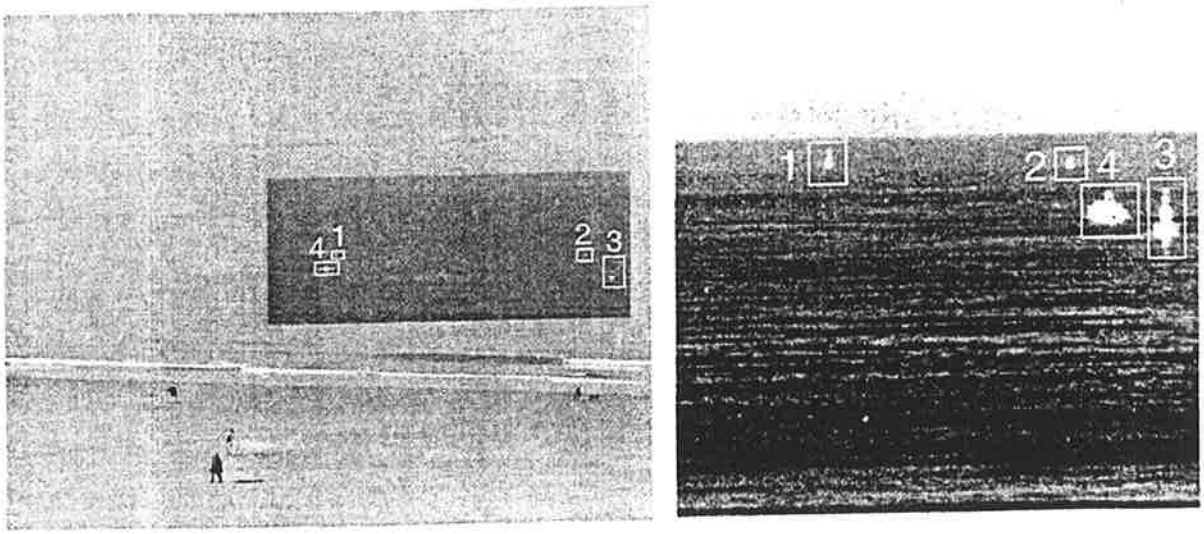

(a) Visual

(b) TIR

Figure 4. The field of view (FOV) of the MWIR polarisation setup in the visual (a) and infrared (b). There are three buoys (number 1 through 3) in the FOV of the MWIR as well as a small motor boat (number 4). In the visual image, this boat is sailing to the right. In the TIR image the boat is sailing to the left and away from the camera. In the visual image the rectangular area, just right of the middle, the contrast is enhanced

image, it shows that the foreground has a lower radiance than the background. Since it is expected that the water has roughly the same temperature, this difference has to be caused by different sky reflection. Apparently the sky reflected in the foreground is colder than the sky reflected in the background. Indeed, in Figure 5 it is noted that the radiance intensity of the sky decreases with elevation angle. The apparent temperature at the horizon is close to the ambient temperature and the ambient temperature is coincidently close to the temperature of the sea water. For higher elevations the radiance intensity of the sky decreases, give rise to larger difference in reflected sky radiance and radiance emitted from the sea surface. This difference in reflected and emitted radiance causes a larger linear polarisation.[7]

The angle of polarisation is around 90 degrees for the sea in the foreground. This means that the angle of maximum polarisation is vertical. This angle corresponds to a situation in which radiance due to emission of the sea surface is larger than the radiance due to reflection of the sky.[7] The sky above the horizon is also polarised. In visual wavelength bands it is known that the sky is largely polarised when the viewing direction is perpendicular to the sun. The phenomenon of infrared polarisation of the sky is analysed in more detail in Section 4.5.

The targets (buoys and boat) also seem to be polarised. This was not expected. In Figure 5 can be seen that the estimated model error is very high. A more detailed analyses of one pixel on the sea surface and one pixel on the boat is given in Figure 6. The intensity of the pixel on the sea surface roughly has the shape of a cosine. There is some noise on each sample as can be expected. However, the pixel on the boat does not have the shape of a cosine. Nonetheless, the resulting model fit is a cosine with an amplitude larger than the amplitude of the pixel on the sea surface.

It is clear that the cosine fit does not match with the intensity of the pixel on the boat. This manifests itself in the larger estimated error σ^2. The reason that the pixel on the boat shows such an erratic behaviour is twofold. First of all, the ship is moving, and hence during the time of 1 second the intensity changes. Secondly, the rotating filter introduces a shift of the complete image, possibly due to an erroneous wedge effect.[11] Though this effect only introduces a shift of an amplitude of about 1 pixel, it is enough for pixels on the boat to wildly vary in intensity. It is not possible to reliably analyse the polarisation of the targets, until a correction of movement (both the filter and the target) is made.

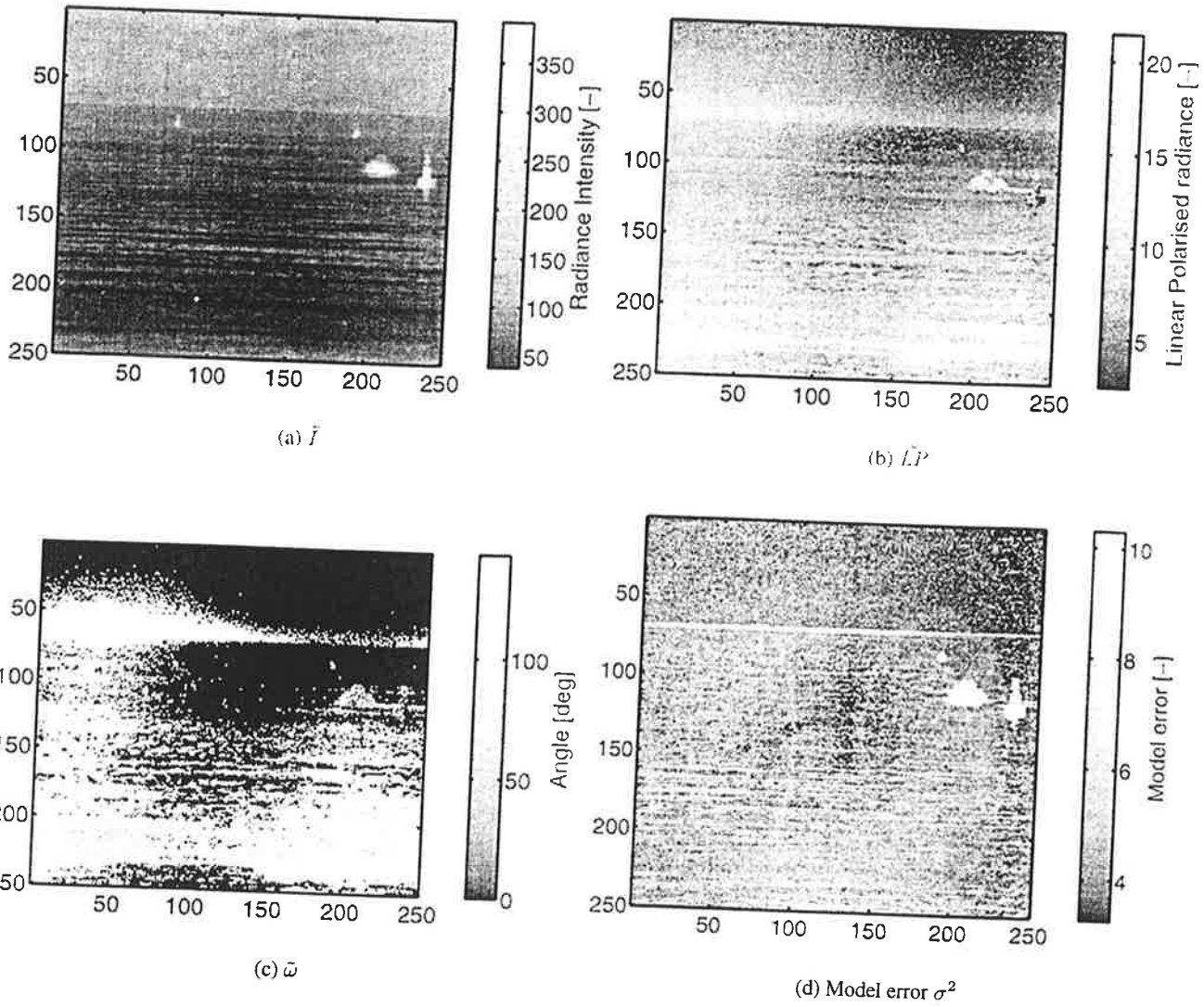

(a) $\tilde{I}$

(b) $\tilde{LP}$

(c) $\tilde{\omega}$

(d) Model error σ^2

Figure 5. One set of images. The radiance intensity image $\tilde{I}$ is given in a). The LP radiation $\tilde{LP}$ is given in b), the angle of polarisation $\tilde{\omega}$ is given in c) and an estimation of the model error is given in d).

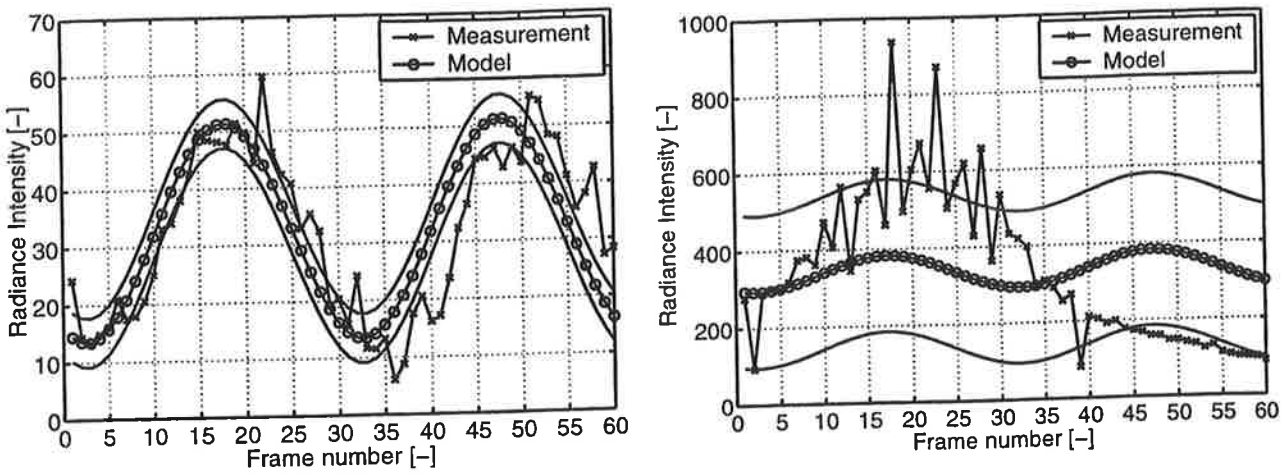

Figure 6. The measured and modelled variation of the radiance of two pixels in time. The solid lines give the boundaries as given by the model RMS. The angle of the principal axis of the polarisation filter ranges from 3 degrees for frame number 1 upto 357 degrees for frame number 60.

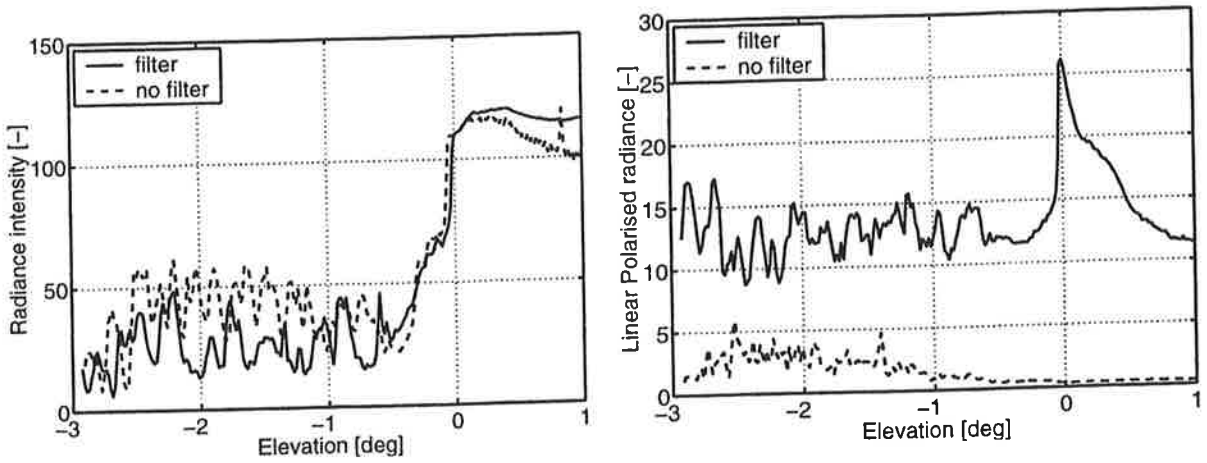

(a) Radiance Intensity

(b) LP radiance

Figure 7. The average radiance intensity and the LP radiance as function of the elevation angle (0 degree is the horizon and positive is above the horizon). The 60 images in each sequence were taken with and without polarisation filter.

4.2. Influence of polarisation filter

Two similar sequences were acquired with and without polarisation filter. This has been performed to verify that the apparent polarisation of the sea is not caused by some other artifacts (for instance movement of the waves, see Section 4.3). In Figure 7 the radiance intensity and the LP radiance are shown for a sequence with and without the filter. The behaviour at the horizon of the radiance is quite similar. However, the radiance of the sea as measured without the filter is higher than when the filter is used.

For the sky we see that this difference is just opposite. The LP radiance, calculated in the same way for both sequences, is much lower when measured without the filter than as measured with the filter. This shows that the filter is working. Movement of waves (which have a period related to the rotation of the filter) causes some 'LP' radiance in the sequence measured without the filter. For the sky this LP radiance is almost zero when measured without the filter, confirming that the apparent LP radiance of the sea, only exists due to movement of the waves.

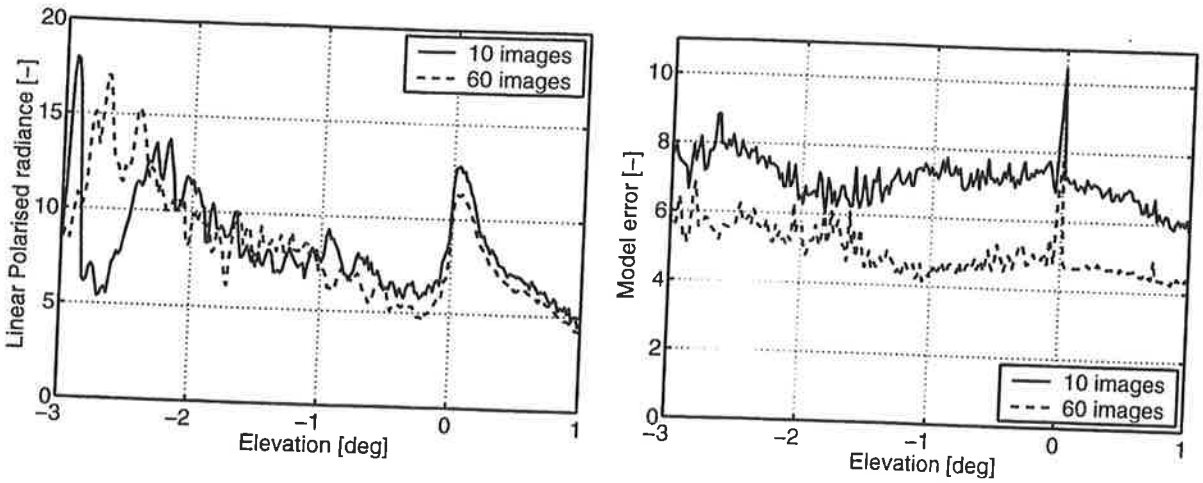

(a) LP radiance

(b) Model error σ^2

Figure 8. The average LP radiance and the model error as function of the elevation angle (0 degree is the horizon and positive is above the horizon). The 10 images were acquired with a rotation speed of 6 rotations per second and the 60 images were acquired at a rotation speed of 1 rotation per second.

4.3. Influence of acquisition speed

The sea background is a dynamic environment (rolling waves, etc). Even though the wind was very moderate, there is some influence to be expected of the acquisition time. The polarisation setup has an adjustable speed. At the lowest speed it rotates at 1 rotation per second (rps) and at high speed it rotates at 6 rps. The integration time is much lower (1 ms) compared to the frame sync (16.7 ms). So the blur due to rotation of the filter during the integration time is small.

In Figure 8 the influence of the rotation speed is shown. Two curves are given: the LP radiance and the model error. The LP radiance is quite similar for both rotation speeds. However, the model error is considerable lower for 1 rps. The sharp peak at 0 degrees elevation (the horizon) is caused by induced movement of the filter, which is not corrected for.

4.4. Temporal variations

It is expected that measurements vary in time. The wind speed and direction may change. So the background structure changes as well as the position of the sun and clouds. To analyse the reproducibility, four measurements of the same scene were acquired in almost 2.5 hours. The average radiance as well as the LP radiance for these four measurements are shown in Figure 9.

The LP radiance shows a dependency with time. The average polarisation of the sea increases with time. This increase is more apparent for the sky (elevation above 0 degree). Most likely this is caused by the different sun position, see Section 4.5. The increase in the average polarisation of the sea probably is caused by an increase of the air temperature.

4.5. Infrared polarisation of the sky

In Section 4.1 we already noticed that the sky above the horizon is polarised. Between 13:09 and 13:24 four sequences of the sky polarisation were recorded in different directions with respect to the direction of the sun. The horizon is identified in these images. The intensity and the LP radiance was averaged over the lines above the horizon. In Figure 10 the intensity and the LP radiation as function of the elevation angle (above the horizon) are shown.

In this figure, both the radiance intensity as well as the LP radiance decreases with elevation. As mentioned before, for visual wavelengths, the maximum polarisation of the sky is found 90 degrees away from the sun (looking perpendicular to the sun direction).[2] However in Figure 10, the maximum polarisation is found at an azimuth of 45 degrees, which is more towards the sun, which implies that the actual angle is slightly higher than 45 degree (due to the elevation of the sun).

For flat surfaces, the amount of LP radiance depends on the radiance difference between source (the sun) and target (the sky), see Equation 1. For visual wavelengths the radiance from the target is negligible, and thus the maximum polarisation is

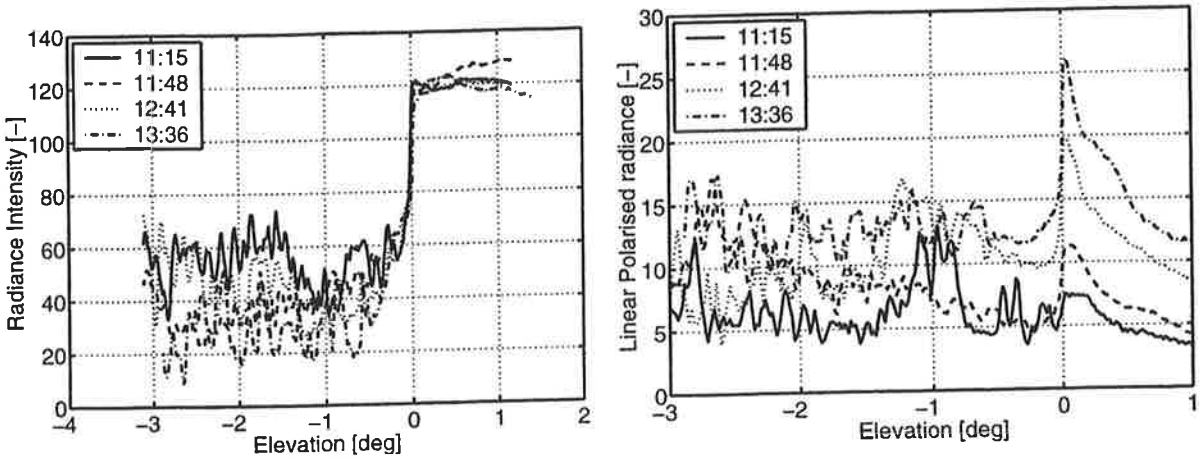

(a) Radiance intensity

(b) LP radiance

Figure 9. The average radiance intensity and the LP radiance as function of the elevation angle (0 degree is the horizon and positive is above the horizon. The four curves show the temporal variation.

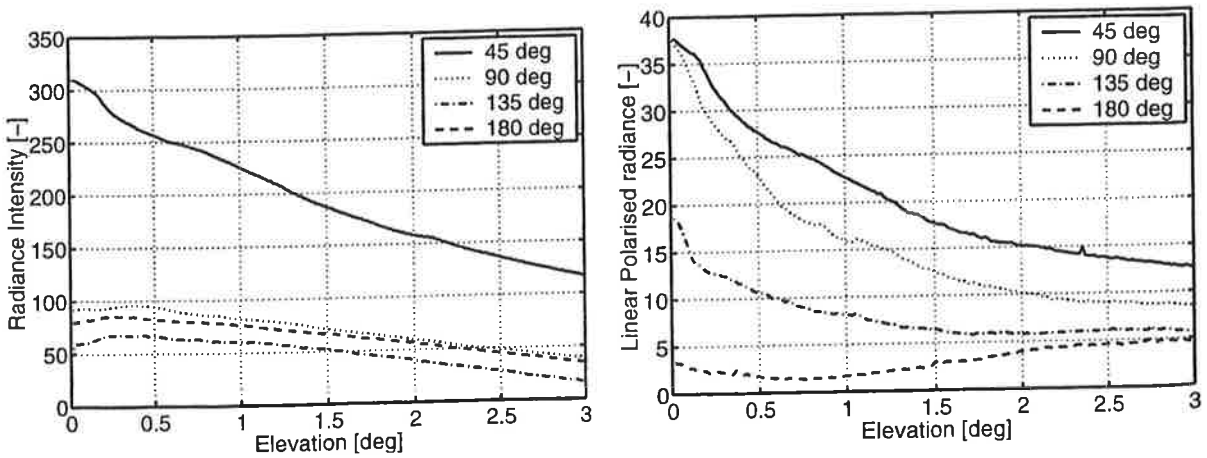

Figure 10. The intensity and LP radiance of the sky as function of the elevation angle above the horizon). Four different orientations (azimuth angles) with respect to the sun were used.

found for the Brewster angle. Due to the emission, the angle of maximum polarisation shifts away from the normal for infrared wavelength bands.[7]

However, the sky is not a flat surface and has to be considered as inhomogeneous substance radiating partly by the constituting molecules and partly by their scattering. The Degree of Linear Polarisation $DoLP(\theta)$ of the sky as function of the angle θ between the observation direction and the position of the sun is given by[2]

$$DoLP(\theta) = \frac{\sin^2\theta}{1+\cos^2\theta} \tag{7}$$

This function has a maximum for $\theta = 90$ degree. This equation is only valid for scattering of monochromatic light on particles that are small compared to the wavelength (also known as Rayleigh scattering). This equation does not take into account the emission from these particles and thus only considers reflection on these particles.

Since the radiance measurement is not calibrated, it is not possible to calculate the degree of polarisation. However, in Figure 10, the radiance intensity is much larger for 45 degree than for the others, so the degree of polarisation for this angle is possibly lower than for 90 degree.

5. CONCLUSIONS

In this paper we have shown a measurement setup that is used for infrared polarisation measurements in a marine environment. We have excluded the supposition that the apparent LP radiance is due to the movement of the waves; their impact is low compared to the polarisation effect.

For these particular measurements there is little difference between slow and fast rotation of the polarisation filter. This is likely caused by the very moderate wind, giving a nearly flat sea surface.

In correspondence with the literature the sea surface appeared polarised. The polarisation angle is vertical, so the emission from the sea surface dominates the reflection of the blue sky. This supposition is supported by the clear blue sky, which is much colder than the sea water. The decrease of polarisation towards the horizon also is an indication for this. Towards the horizon, the sources that reflect on the sea surface have a temperature closer to the sea water temperature than the sources reflecting (the blue sky) under steeper angles.

Due to induced movements by the filter as well as movement of the targets, it was not possible to reliably measure the polarisation of the targets. With our current processing the targets appear to be significantly linearly polarised, but also the model error is large.

The sky above the horizon is linearly polarised. The amount of polarisation depends on the view angle with respect to the sun direction. The maximum LP radiance was found for an azimuth angle of 45 degrees with the sun direction (i.e. partly looking towards the sun direction). In visual wavelength bands, the maximum degree of polarisation is expected to be found at 90 degrees. However, the degree of polarisation in these measurements could not be calculated. The measured polarisation decreases sharply with the elevation angle. This may be caused by the atmospheric conditions (it was a bit hazy above the sea).

For future work, it is recommended to calibrate the system, so that the absolute radiance intensity can be measured. This will allow to calculate the degree of polarisation as function of the viewing angle relative to the sun direction. Furthermore, there should be a correction for the movements of the targets as well as induced movement of the rotating filter.

REFERENCES

1. L. S. Balfour, Y. Bushlin, and N. Brandman. Polarization signatures of man made objects in the SW infrared spectrum band. In W. R. Watkins and D. Clement, editors, *Proc. SPIE Vol. 3375, Targets and Backgrounds: Characterization and Representation IV*, pages 48–53, Orlando (FL), USA, Apr. 1998.
2. M. Born and E. Wolf. *Principles of Optics*. Pergamon Press, second edition, 1964.
3. A. W. Cooper, E. C. Crittenden, E. A. Milne, P. L. Walker, E. Moss, and D. J. Gregoris. Mid- and far-infrared measurements of sun glint from the sea surface. In L. Estep, editor, *Proc. SPIE Vol. 1749, Optics of the Air-Sea Interface: Theory and Measurement*, pages 176–185, Dec. 1992.
4. A. W. Cooper, W. J. Lentz, P. L. Walker, and P. M. Chan. Infrared polarization measurements of ship signatures and background contrast. In W. R. Watkins and D. Clement, editors, *Proc. SPIE Vol. 2223, Characterization and Propagation of Sources and Backgrounds*, pages 300–309, Orlando (FL), USA, Apr. 1994.
5. A. W. Cooper, W. J. Lentz, P. L. Walker, and P. Chan. Polarization enhancement of contrast in infrared ship/background imaging. In *AGARD CP576, Propagation Assessment in Coastal Environments*, pages 26.1–26.10, Bremerhaven, Germany, Sept. 1994.
6. A. W. Cooper, W. J. Lentz, and P. L. Walker. Infrared polarization ship images and contrast in the maptip experiment. In J. C. Dainty and L. R. Bissonnette, editors, *Proc. SPIE Vol. 2828, Image Propagation through the Atmosphere*, pages 85–96, Denver (CO), USA, Aug. 1996.
7. F. Cremer, W. de Jong, and K. Schutte. Infrared polarization measurements of surface and buried anti-personnel landmines. In A. C. Dubey, J. F. Harvey, J. T. Broach, and V. George, editors, *Proc. SPIE Vol. 4394, Detection and Remediation Technologies for Mines and Minelike Targets VI*, Orlando (FL), USA, Apr. 2001.
8. D. J. Gregoris, S. K. Yu, A. W. Cooper, and E. A. Milne. Dual-band infrared polarization measurements of sun glint from the sea surface. In D. Clement and W. R. Watkins, editors, *Proc. SPIE Vol. 1687, Characterization, Propagation, and Simulation of Sources and Backgrounds II*, pages 381–391, Sept. 1992.
9. E. Hecht. *Optics*. Addison-Wesley publishing company, Reading (MA), USA, second edition, 1987.
10. F. J. Iannarilli, Jr, J. A. Shaw, S. H. Jones, and H. E. Scott. Snapshot LWIR hyperspectral polarimetric imager for ocean surface sensing. In D. H. Goldstein, D. B. Chenault, W. G. Egan, and M. J. Duggin, editors, *Proc. SPIE Vol. 4133, Polarization Analysis, Measurement, and Remote Sensing III*, San Diego (CA), USA, July 2000.
11. W. de Jong, F. Cremer, K. Schutte, and J. Storm. Usage of polarisation features of landmines for improved automatic detection. In A. C. Dubey, J. F. Harvey, J. T. Broach, and R. E. Dugan, editors, *Proc. SPIE Vol. 4038, Detection and Remediation Technologies for Mines and Minelike Targets V*, pages 241–252, Orlando (FL), USA, Apr. 2000.
12. R. Neuwirth and K. Stein. Polarization and turbulence effects measured at the Nettuno trials, Italy 1998. In J. D. Gonglewski, G. Kamerman, A. Kohnle, U. Schreiber, and C. Werner, editors, *Proc. SPIE Vol. 4167, Atmospheric Propagation, Adaptive Systems, and Laser Radar Technology for Remote Sensing*, Barcelona, Spain, Sept. 2000.
13. P. L. Walker, W. J. Lentz, and A. W. Cooper. Atmospheric and sea state dependence of polarized infrared contrast. In W. R. Watkins and D. Clement, editors, *Proc. SPIE Vol. 2469, Targets and Backgrounds: Characterization and Representation*, pages 393–403, Orlando (FL), USA, Apr. 1995.